THE JOURNAL OF BIOLOGICAL CHEMISTRY VOL. 290, NO. 8, pp. 4631–4646, February 20, 2015

Microtubule-associated Proteins 1 (MAP1) Promote Human Immunodeficiency Virus Type I (HIV-1) Intracytoplasmic Routing to the Nucleus

Received for publication, September 19, 2014, and in revised form, December 8, 2014 Published, JBC Papers in Press, December 11, 2014, DOI 10.1074/jbc.M114.613133

Juliette Fernandez[‡1], Débora M. Portilho[‡1], Anne Danckaert[§], Sandie Munier[¶], Andreas Becker[‡], Pascal Roux[§], Anaba Zambo[‡], Spencer Shorte[§], Yves Jacob[¶], Pierre-Olivier Vidalain[‖], Pierre Charneau[**], François Clavel[‡], and Nathalie J. Arhel[‡2]

*From [‡]INSERM U941, Institut Universitaire d'Hématologie de l'Hôpital Saint-Louis, 75010 Paris, France, [§]Imagopole, Institut Pasteur, 75015 Paris, France, the [¶]Département de Virologie, Unité de Génétique Moléculaire des Virus à ARN, Université Paris Diderot, CNRS UMR3569, Institut Pasteur, 75015 Paris, France, [‖]Unité de Génomique Virale et Vaccination, CNRS UMR3569, Institut Pasteur, 75015 Paris, France, and the **Unité de Virologie Moléculaire et Vaccinologie, Institut Pasteur, 75015 Paris, France*

Background: During infection, HIV uses the host cytoskeleton to traffic across the cytoplasm to the nucleus where it integrates its genome.
Results: Microtubule-associated proteins (MAP1A and MAP1S) promote HIV trafficking to the nucleus.
Conclusion: MAP1 proteins help tether viral capsids to microtubules.
Significance: This is the first description of HIV-microtubule interactions that contribute to HIV trafficking to the nucleus.

After cell entry, HIV undergoes rapid transport toward the nucleus using microtubules and microfilaments. Neither the cellular cytoplasmic components nor the viral proteins that interact to mediate transport have yet been identified. Using a yeast two-hybrid screen, we identified four cytoskeletal components as putative interaction partners for HIV-1 p24 capsid protein: MAP1A, MAP1S, CKAP1, and WIRE. Depletion of MAP1A/MAP1S in indicator cell lines and primary human macrophages led to a profound reduction in HIV-1 infectivity as a result of impaired retrograde trafficking, demonstrated by a characteristic accumulation of capsids away from the nuclear membrane, and an overall defect in nuclear import. MAP1A/MAP1S did not impact microtubule network integrity or cell morphology but contributed to microtubule stabilization, which was shown previously to facilitate infection. In addition, we found that MAP1 proteins interact with HIV-1 cores both *in vitro* and in infected cells and that interaction involves MAP1 light chain LC2. Depletion of MAP1 proteins reduced the association of HIV-1 capsids with both dynamic and stable microtubules, suggesting that MAP1 proteins help tether incoming viral capsids to the microtubular network, thus promoting cytoplasmic trafficking. This work shows for the first time that following entry into target cells, HIV-1 interacts with the cytoskeleton via its p24 capsid protein. Moreover, our results support a role for MAP1 proteins in promoting efficient retrograde trafficking of HIV-1 by stimulating the formation of stable microtubules and mediating the association of HIV-1 cores with microtubules.

During their replication cycle, most enveloped viruses must move from the cell surface membrane to the compartments containing the machinery for their replication and back to the plasma membrane for assembly and release. Passive diffusion through the cytoplasm is very ineffective and rarely leads to the required destination. Therefore, viruses have evolved mechanisms enabling them to "hijack" the cellular cytoskeleton, normally destined for the transport of cellular proteins and vesicles, for their active transport within infected cells (1). During the early phase of HIV-1 infection, incoming virions fuse with the host cell membrane, allowing the viral complex referred to as the reverse transcription complex (RTC)[3] to be transported through the cytoplasm toward the nucleus. After crossing the cortical actin meshwork, HIV-1 uses both the microtubule and microfilament networks to traffic toward the nucleus (2, 3). Genome-wide RNA interference-based screens have identified numerous tubulin- and actin-associated proteins that may contribute to efficient infection (4–6). However, as HIV interacts with the cytoskeleton at multiple points in its replication cycle and remodels the cytoskeleton to promote viral replication, it is unclear which cellular factors are specifically involved in trafficking.

The nature of the HIV RTC that traffics along the cytoskeleton to reach the nucleus is currently poorly characterized. After viral cell entry, the capsid structure of HIV disassembles to allow infection to proceed; however, the timing and location of this uncoating are still uncertain. Work based on capsid mutants or chimeras shows a functional link between HIV-1 capsid and nuclear import via the nuclear pore (7–10), and HIV-1 cores have been shown to dock at the nuclear pore and

[1] Both authors contributed equally.
[2] To whom correspondence should be addressed: INSERM U941, Génétique des Virus et Pathogénèse des Maladies Virales, Institut Universitaire d'Hématologie (IUH), Hôpital St Louis, 1 Ave. Claude Vellefaux, 75010 Paris, France. Tel.: 33-1-57276756; Fax: 33-1-57276804; E-mail: nathalie.arhel@inserm.fr.

[3] The abbreviations used are: RTC, reverse transcription complex; VSV-G, vesicular stomatitis virus glycoprotein; dpt, days post-transduction; hpi, hours post-infection; m.o.i., multiplicity of infection; KD, knockdown; LV, lentiviral vector; LRT, late reverse transcript; ANOVA, analysis of variance; MAP, microtubule-associated protein; MTT, 3-(4,5-dimethylthiazol-2-yl)-2,5-diphenyltetrazolium bromide; NT, non-transduced.

interact directly with Nup358/RanBP2 (11–13). Evidence further suggests that uncoating is closely coordinated with the reverse transcription of the viral genome. Acceleration of TRIM5α-mediated uncoating correlates with inhibition of reverse transcription (14–17), mutations in capsid proteins that affect the stability of the HIV-1 core interfere with reverse transcription (18, 19), and inhibition of reverse transcription delays or prevents uncoating (11, 20). Recent work shows that the stability of the HIV capsid is key in preventing the sensing of viral DNA by cyclic GMP-AMP synthase (cGAS) (21, 22) and in dictating susceptibility to Mx2 after successful reverse transcription (23–25), suggesting that the capsid remains intact until the viral DNA is fully synthesized, which is estimated to occur at 4–12 h post-infection and up to 16–24 h in primary macrophages (11, 26–28). However, there is also evidence that uncoating or partial uncoating can happen earlier, within 30–45 min of infection (20, 29), which may be key in establishing productive infection, for instance by eliminating suboptimal complexes or, on the contrary, priming complexes for full uncoating at a later time.

Although some uncoating or partial uncoating can happen at the early post-infection stage, the importance of the viral capsid for efficient reverse transcription and its presence at the nuclear pore implies that many complexes that traffic along the cytoskeleton toward the nucleus still contain capsid. Because the capsid sequesters all other viral components remaining after cell entry until full uncoating, we hypothesized that the viral component that interacts with the cytoskeleton for active transport toward the nucleus might be the viral capsid. Here, we report the interaction of HIV-1 capsid cores with human MAP1A and MAP1S, two microtubule-associated proteins. This suggested a potential role for MAP1A and MAP1S in HIV-cytoskeleton interactions and viral transport, which we decided to investigate further. Depletion of MAP1A or MAP1S in indicator cell lines and primary human macrophages disrupted HIV-1 infection by hampering the efficient trafficking of incoming HIV-1 complexes to the nucleus. MAP1A/MAP1S did not impact microtubule network integrity or cell morphology but did stabilize microtubules in primary human macrophages. HIV-1 capsid association with both dynamic and stable microtubules was lost upon MAP1 depletion, suggesting that MAP1 proteins facilitate the tethering of HIV-1 complexes to microtubules. Our work shows for the first time that following entry into target cells, HIV-1 interacts with the cytoskeleton via its p24 capsid protein, supporting a role for MAP1A proteins in promoting the efficient retrograde trafficking of HIV-1 by stimulating the formation of stable microtubules and mediating their association with HIV-1 cores.

EXPERIMENTAL PROCEDURES

Yeast Two-hybrid Assay—The p24 constructs were cloned into pDONR207, fused to the GAL4 DNA binding domain in pGBKT7 (pGBKT7-p24), and used to screen the human brain Matchmaker cDNA library (Clontech). The complexity of this cDNA library was about 5 × 106 independent inserts with an average size of 1.5 kb. The cDNA library was cloned into the pACT2 vector (Clontech), and then transformed into the Y187 yeast strain (MATα ura3–52 his3–200 ade2–101 trp1–901 leu2–3112 gal4Δ mel gal80Δ URA3::GAL1UAS-GAL1TATA-lacZ) using a standard large scale transformation procedure to obtain about 107 individual yeast colonies corresponding to a 2-fold coverage of the cDNA library. In parallel, pGBKT7-p24 constructs were established in the AH109 yeast strain (MATα trp1–901 leu2–3112 ura3–52 his3–200 gal4Δ gal80Δ LYS2::GAL1UAS-GAL1TATA-HIS3 GAL2UASGAL2- TATA-ADE2 URA3::MEL1UAS-MEL1TATA-lacZ). p24 baits were used to screen the cDNA library by mating. A mix of AH109 and Y187 yeasts were plated for 4 h at 30 °C on solid medium containing yeast extract, peptone, and dextrose at pH 3.5 (YCM). Mated yeast cells were grown for 5 days on synthetic dextrose medium lacking tryptophan, leucine, and histidine and containing 20 mM 3-aminotriazole to select for diploids that showed elevated expression of the GAL1::HIS3 Y2H reporter. The prey cDNAs corresponding to HIS3 positive colonies were PCR amplified and sequenced, and the resulting sequences were analyzed with BLAST.

Cells—P4-CCR5 reporter cells used were HeLa CD4+ CXCR4+ CCR5+ carrying the *LacZ* gene under the control of the HIV-1 LTR promoter (30). The 293T cells are human embryonic kidney cells (ATCC). Citrate human blood was obtained from healthy donors (Etablissement Français du Sang). Monocytes were isolated using adherence on plastic (45 min) after Ficoll gradient and were differentiated to macrophages by incubation for 7–10 days with 50 ng/ml GM-CSF (Gentaur).

Viruses—LAI and NL43 human immunodeficiency viruses were produced by transient transfection of 293T cells using calcium phosphate precipitation with a wild-type *env* proviral plasmid or Δ*env* construct co-transfected with the vesicular stomatitis virus glycoprotein (VSV-G) envelope expression plasmid pHCMV-G (31). Viruses were harvested at 48 h after transfection. The virus yield was measured by p24 ELISA according to the manufacturer's instructions (PerkinElmer Life Sciences).

Lentiviral Vector-shRNA Construction, Production, and Transduction—Complementary oligonucleotides coding for shRNAs were annealed and cloned into BglII/HindIII of pSUPER (Oligo-Engine) downstream of the H1 promoter. The H1-shRNA cassette was then inserted into a polylinker within the U3 region of the TRIP-CMV-eGFP vector (32). Lentiviral vector (LV)-shRNAs were produced by transient co-transfection of 293T cells with the vector, encapsidation (pCMVΔR 8.74), and VSV-G plasmids. Vectors were harvested 48 h post-transfection and concentrated by ultracentrifugation for 1 h at 64,000 × *g* (Beckman Coulter) at 4 °C. LV-shRNAs were titered in P4-CCR5 cells using flow cytometry to assess GFP expression at 4 days post-transduction (dpt). P4-CCR5 cells and primary human macrophages (4×10^6) were transduced with LV-shRNA at m.o.i. 50. All knockdown (KD) cells were used at 3 dpt.

Reverse Transfection of siRNAs—P4-CCR5 cells were reverse transfected with final concentrations of 10 and 50 nM siRNA (Dharmacon) in a final volume of 600 μl. Scramble siRNA was the Dharmacon ON-TARGET plus non-targeting pool. Briefly, 6 and 30 pmol of siRNAs were diluted in 90 μl of Opti-MEM. Then, Lipofectamine RNAiMAX (Invitrogen) was diluted 1:10 in Opti-MEM, and 10 μl was added to the 90 μl of diluted siRNAs. The transfection mix was incubated at room temper-

ature for 20 min in a 24-well plate. P4-CCR5 (30,000) cells were diluted in 500 μl of DMEM plus 10% FCS without antibiotics, and 500 μl of cell suspension was added to the siRNA mix. Incubation was for 48 h at 37 °C.

RT-PCR—At 48 h after reverse transfection with siRNAs, or 72 h after transduction with LV-shRNAs, total RNA was isolated from P4-CCR5 cells using an RNeasy mini kit according to the manufacturer's instructions (Qiagen). RT-PCR was carried out by using a One-step RT-PCR kit (Qiagen) according to the manufacturer's instructions.

β-Galactosidase and Bradford Assay—A β-galactosidase assay was performed 48 h post-infection (hpi) in indicator P4-CCR5 cells according to the manufacturer's instructions (Roche Applied Science). β-Galactosidase activity was normalized for protein concentration by the Bradford assay.

Quantitative PCR—Total cellular DNA was isolated 24 hpi using the QIAamp DNA micro kit (Qiagen). Two long-terminal repeat (2-LTR)-containing circles were detected with primers MH535/536 and probe MH603 (33), using as the standard curve the pUC2LTR plasmid, which contains the HIV-1 2-LTR junction. Reactions were normalized by amplification of the late reverse transcript with primers MH531/532 and probe LRT-P (33). Alu-PCR was performed according to a protocol adapted from Brussel and Sonigo (34) as published previously (12).

Antibodies and Stains—The primary antibodies used were mouse monoclonal anti-β-actin, mouse monoclonal anti-α-tubulin, and acetylated tubulin (Sigma), rabbit polyclonal anti-detyrosinated tubulin (EMD Millipore), mouse monoclonal anti-p24 clone 183-H12-5C (NIH AIDS Reagent Program), rabbit anti-cyclophilin A (Cell Signaling, Denver, CO), mouse monoclonal anti-FLAG, rabbit polyclonal anti-MAP1A, and -MAP1S, and rat monoclonal anti-tubulin (YL1/2) (Abcam). Secondary antibodies were goat anti-mouse and anti-rabbit HRP conjugates (Thermo Fisher Scientific, Rockford, IL), goat anti-rabbit IgG (H+L) Alexa Fluor 488 (Molecular Probes), and goat anti-mouse Cy3 (GE Healthcare). Actin cytoskeleton was labeled with rhodamine phalloidin (Molecular Probes) staining, and nuclei were stained with Hoechst (Invitrogen).

Microscopy Immunolabeling—Cultures were rinsed with PBS and fixed with 4% paraformaldehyde in PBS for 10 min at room temperature. They were then permeabilized with 0.5% Triton X-100 in PBS three times for 10 min. The same solution was used for all subsequent washing steps. Cells were incubated with primary antibodies for 1 h at 37 °C. After incubation, cells were washed for 30 min and incubated with Alexa Fluor- or Cy3-conjugated secondary antibodies for 1 h at 37 °C, and the nuclei were labeled with Hoechst dye.

Imaging and Data Analysis—The image acquisition of P4-CCR5 was carried out using a confocal microscope (Zen 2012 LSM700, Zeiss) with a Plan-Apochromat ×63/NA 1.4 objective, and 16-bit z-stack random field images were acquired as 1024 × 1024 pixels with a line averaging of 2. To perform a statistical analysis of capsid position in primary macrophages, we used the Cell Voyager spinning disk confocal system (CV1000, Yokogawa) for high-throughput mosaic analysis with an Olympus microscope (UPLSAPO ×40/NA 1.3). The sample area was acquired as a square of 10 × 10 fields of view (920 × 920 pixels for each) for each condition. In total ~600–700 macrophages were acquired per condition, and only those that were GFP positive (*i.e.* shRNA transduced) were analyzed, corresponding to ~10% of the cells. In these two acquisition approaches, three signals, Hoechst, eGFP, and Cy3, were detected over multiple z-slices ($z = 8–12$). For each z-position, the CV1000 reconstructed mosaic or random field from LSM700 image analysis was carried out using Acapella software (PerkinElmer Life Sciences). Cells were analyzed over a constant volume of four z-slices for P4-CCR5 and five z-slices for macrophages, selected around the focal plane of the center of each nucleus. The script was subdivided into three object subroutines segmenting successively the nucleus, the cytoplasm, and the spots within the perinuclear regions of each cell by z-position. Statistical analyses (one-way ANOVA with Dunnett's multiple comparisons test) were performed using Prism 6 (GraphPad).

Capsid Binding Assay—The pCiNeo3×FLAG plasmid was used for cloning FLAG fusions of candidate proteins under the control of the CMV promoter. The cDNA of candidate p24 CA interactors were transferred from the pENTR plasmid to the pCiNeo3×FLAG plasmid as a fusion dowstream of the 3×FLAG motif by *in vitro* recombination (LR cloning reaction, Gateway Technology, Invitrogen). Cells were either transfected at 60–80% confluency with FLAG pCiNeo3× constructs or left untransfected. After 24 h the cells were lysed in ice-cold cell lysis buffer (5 mM Tris, pH 8, 150 mM NaCl, 5 mM EDTA, and 0.01% Nonidet P-40) for 40 min on ice. The lysate was then briefly vortexed, and cell debris was cleared by centrifugation at 13,000 rpm at 4 °C for 30 min. HIV-1 capsids were prepared by centrifugation through a sucrose cushion by overlaying on ice in 1 ml of 50% sucrose (PBS) with 1 ml of 10% sucrose plus 0.1% Triton X-100. As a negative control, a sucrose cushion without Triton was produced. Viral supernatants (500 μl) were layered onto the 10% phase and centrifuged at 32,500 rpm for 2 h at 4 °C (SW55Ti rotor). After centrifugation, the presence of intact capsids (in the pellet) and soluble capsid (in 250 μl from the top of the supernatant) was measured by p24 ELISA. The presence of intact cores in the pellet was confirmed by negative staining followed by transmission electron microscopy (data not shown). Clarified cell lysate (120 μl) was incubated with capsids (100 μl) for 1 h on ice. Capsids were then ultracentrifuged at 15,000 rpm (TLS 55 rotor) at 4 °C for 30 min. After centrifugation the pellets were resuspended in 150 μl of ice-cold PBS and analyzed by Western blotting.

Duolink Proximity Ligation Assay—Paraformaldehyde-fixed P4-CCR5 cells were preincubated with blocking agent for 1 h. After washing in PBS for 10 min, cells were incubated with primary anti-MAP1A and anti-p24 antibodies for 1 h in a preheated humidity chamber at 37 °C. Slides were washed three times in PBS for 10 min and then they were incubated with Duolink proximity ligation assay probes (Olink Bioscience) diluted in the blocking agent (1:5) for 1 h in a preheated humidity chamber at 37 °C. Ligation of the connector oligonucleotides, rolling circle amplification, and detection of the amplified DNA products were done with Duolink Detection Reagents Red according to the manufacturer's instructions. Nuclei were labeled with Hoechst dye.

TABLE 1

HIV-1 p24 interactors identified by yeast two-hybrid screen

The gene identifier number, the number of isolated clones, and the full name of the candidate are indicated. The candidates investigated further in this study appear in bold.

Gene symbol	Gene ID	Occurrence	Description
AGPS	8540	2	Alkyldihydroxyacetonephosphate synthase, peroxisomal precursor (EC 2.5.1.26) (Alkyl-DHAP synthase) (Alkylglycerone-phosphate synthase) (Source:Uniprot/SWISSPROT;Acc:O00116)
ANKRD35	148741	1	Ankyrin repeat domain 35 (Source:RefSeq_peptide;Acc:NP_653299)
ATP5C1	509	1	ATP synthase γ-chain, mitochondrial precursor (EC 3.6.3.14) (Source:Uniprot/SWISSPROT;Acc:P36542)
MAP1S	**55201**	**3**	**BPY2-interacting protein 1 (Source:RefSeq_peptide;Acc:NP_060644)**
CNRIP1	25927	7	Cannabinoid receptor-interacting protein 1
CPT1C	126129	1	Carnitine *O*-palmitoyltransferase I, brain isoform (EC 2.3.1.21) (carnitine palmitoyltransferase 1C) (CPT IC) (Source:Uniprot/SWISSPROT;Acc:Q8TCG5)
COPS5	10987	5	COP9 signalosome complex subunit 5 (EC 3.4.-.-) (signalosome subunit 5) (SGN5) (Jun activation domain-binding protein 1) (Source:Uniprot/SWISSPROT;Acc:Q92905)
COX7C	1350	1	Cytochrome *c* oxidase polypeptide VIIc, mitochondrial precursor (EC 1.9.3.1). (Source:Uniprot/SWISSPROT;Acc:P15954)
MT-CO_2	4513	1	Cytochrome *c* oxidase subunit 2 (EC 1.9.3.1) (cytochrome *c* oxidase polypeptide II) (Source:Uniprot/SWISSPROT;Acc:P00403)
GPC1	2817	1	Glypican-1 precursor (Source:Uniprot/SWISSPROT;Acc:P35052)
HTT	3064	1	Huntingtin (Huntington disease protein) (HD protein) (Source:Uniprot/SWISSPROT;Acc:P42858)
IPO5	3843	1	Importin β-3 (karyopherin β-3) (Ran-binding protein 5) (RanBP5) (Source:Uniprot/SWISSPROT;Acc:O00410)
LDHB	3945	1	L-Lactate dehydrogenase B chain (EC 1.1.1.27) (LDH-B) (LDH heart subunit) (LDH-H) (Source:Uniprot/SWISSPROT;Acc:P07195)
MT2A	4502	3	Metallothionein-2 (MT-2) (metallothionein-II) (MT-II) (metallothionein-2A) (Source:Uniprot/SWISSPROT;Acc:P02795)
MAP1A	**4130**	**7**	**Microtubule-associated protein 1A (MAP 1A) (proliferation-related protein p80) (contains MAP1 light chain LC2) (Source:Uniprot/SWISSPROT;Acc:P78559)**
MT-ND2	4536	1	NADH-ubiquinone oxidoreductase chain 2 (EC 1.6.5.3) (NADH dehydrogenase subunit 2) (Source:Uniprot/SWISSPROT;Acc:P03891)
NUB1	51667	1	NEDD8 ultimate buster 1 (NY-REN-18 antigen). (Source:Uniprot/SWISSPROT;Acc:Q9Y5A7)
PANK1	53354	1	Pantothenate kinase 1 (EC 2.7.1.33) (pantothenic acid kinase 1) (hPanK1) (hPanK) (Source:Uniprot/SWISSPROT;Acc:Q8TE04)
PPIB	5479	1	Peptidyl-prolyl cis-trans isomerase B precursor (EC 5.2.1.8) (PPIase) (Rotamase) (cyclophilin B) (*S*-cyclophilin) (SCYLP) (CYP-S1) (Source:Uniprot/SWISSPROT;Acc:P23284)
PPIE	10450	1	Peptidyl-prolyl cis-trans isomerase E (EC 5.2.1.8) (PPIase E) (Rotamase E) (cyclophilin E) (cyclophilin 33) [Source:Uniprot/SWISSPROT;Acc:Q9UNP9]
PPIF	10105	1	Peptidyl-prolyl cis-trans isomerase, mitochondrial precursor (EC 5.2.1.8) (PPIase) (rotamase) (cyclophilin F) (Source:Uniprot/SWISSPROT;Acc:P30405)
PCBP1	5093	2	Poly(rC)-binding protein 1 (α-CP1) (hnRNP-E1) (nucleic acid-binding protein SUB2.3) (Source:Uniprot/SWISSPROT;Acc:Q15365)
RBBP6	5930	1	Retinoblastoma-binding protein 6, isoform 2 (Source:RefSeq_peptide;Acc:NP_061173)
PPP2R5A	5525	1	Serine/threonine-protein phosphatase 2A, 56-kDa regulatory subunit α isoform (PP2A, B subunit, B′ α isoform) (PP2A, B subunit, B56α isoform) (PP2A, B subunit, PR61 α isoform) (PP2A, B subunit, R5 α isoform) (Source:Uniprot/SWISSPROT;Acc:Q15172)
PON3	5446	1	Serum paraoxonase/lactonase 3 (EC 3.1.1.-). (Source:Uniprot/SWISSPROT;Acc:Q15166)
SLC24A1	9187	1	Sodium/potassium/calcium exchanger 1 (Na(+)/K(+)/Ca(2+)-exchange protein 1) (retinal rod Na-Ca+K exchanger). (Source:Uniprot/SWISSPROT;Acc:O60721)
SRI	6717	2	Sorcin (22 kDa protein) (CP-22) (V19) (Source:Uniprot/SWISSPROT;Acc:P30626)
SF1	7536	2	Splicing factor 1 (Zinc finger protein 162) (transcription factor ZFM1) (zinc finger gene in MEN1 locus) (mammalian branch point-binding protein mBBP) (BBP) (Source:Uniprot/SWISSPROT;Acc:Q15637)
TSPAN13	27075	2	Tetraspanin-13 (Tspan-13) (transmembrane 4 superfamily member 13) (Tetraspan NET-6) (Source:Uniprot/SWISSPROT;Acc:O95857)
TBCB	**1155**	**3**	**Tubulin-specific chaperone B (tubulin folding cofactor B) (cytoskeleton-associated protein 1) (cytoskeleton-associated protein CKAPI) (Source:Uniprot/SWISSPROT;Acc:Q99426)**
WIPF2	**147179**	**1**	**WIP-related protein (WASP-interacting protein-related protein) (WIP- and CR16-homologous protein) (Source:Uniprot/SWISSPROT;Acc:Q8TF74)**
ZNF26	7574	1	Zinc finger protein 26 (zinc finger protein KOX20) (Source:Uniprot/SWISSPROT;Acc:P17031)
ZNF333	84449	1	Zinc finger protein 333 (Source:Uniprot/SWISSPROT;Acc:Q96JL9)
RLF	6018	2	Zinc finger protein Rlf (rearranged L-*myc* fusion gene protein) (Zn-15- related protein) (Source:Uniprot/SWISSPROT;Acc:Q13129)

RESULTS

MAP1A and MAP1S Promote the Early Steps of HIV-1 Infection—As a result of yeast two-hybrid screens that aimed at mapping HIV-host interactions at the protein level, four cytoskeleton-associated factors, namely MAP1A, MAP1S (BPY2), CKAP1 (CoB), and WIRE (WICH/WIPF2), were identified as putative partners of HIV-1 p24 capsid protein (Table 1). MAP1A and MAP1S belong to the same MAP1 family of proteins, which bind along the length of the microtubules with the primary role of stabilizing the microtubules (35). MAP1 proteins are translated as larger proteins that are proteolytically cleaved into heavy chains, MAP1A-HC (350 kDa) and MAP1S-HC (100 kDa), and light chains, MAP1A-LC2 (28 kDa) and MAP1S-LC (26 kDa). CKAP1 (cytoskeleton-associated protein) is a 38-kDa protein that binds to folded α-tubulin and promotes tubulin heterodimer quaternary structure formation, necessary for microtubule polymerization (36). Finally, WIRE belongs to the verprolin family of F-actin-binding proteins that regulate actin filament polymerization following signaling via WASPs (Wiskott-Aldrich syndrome protein) and Arp2/3 (37). This suggested that MAP1A, MAP1S, CKAP1, and WIRE might play a role in HIV-cytoskeleton interactions and viral transport, which we decided to investigate further.

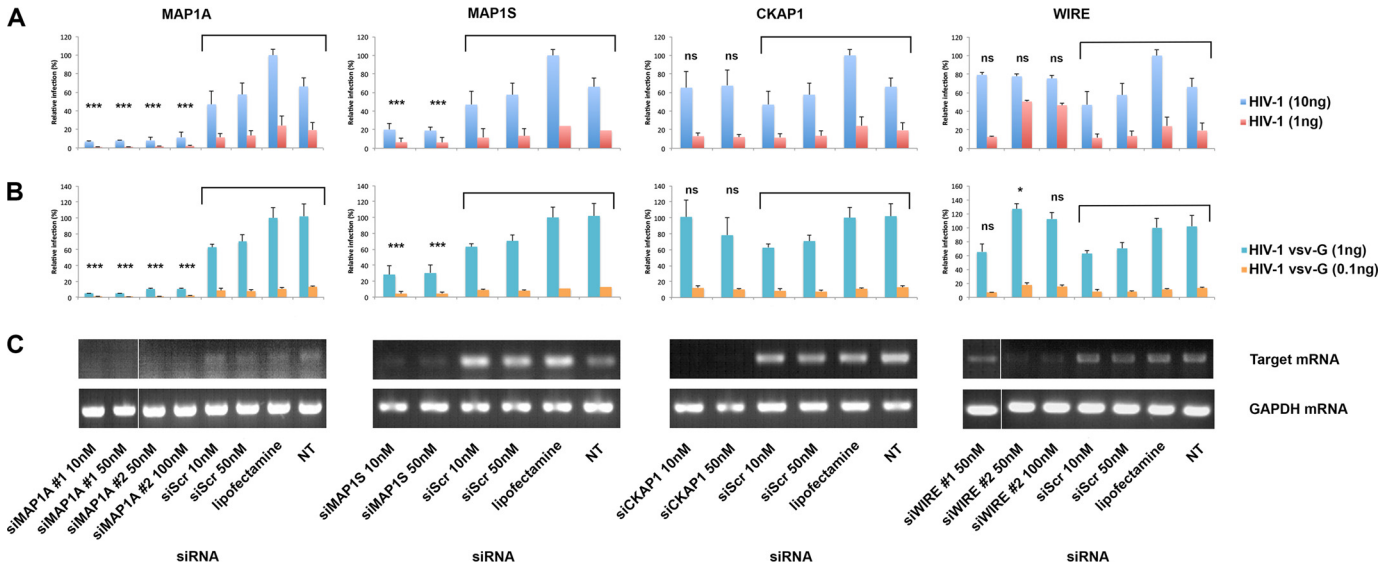

FIGURE 1. **MAP1 proteins are required for efficient HIV-1 infection.** P4-CCR5 cells were infected with two different doses of HIV-1 (10 and 1 ng of p24/well) (*A*) and VSV-G-pseudotyped HIV-1 (1 and 0.1 ng of p24) (*B*). Infectivity was assessed by β-galactosidase activity at 48 hpi and normalized by Bradford assay for each well. Results show the mean of three independent experiments carried out in duplicate, with lipofection without siRNA and 10 ng infection set as 100%. For this point, the raw values were ~300,000 relative light units/s on average. *ns*, not significant. *C*, mRNA levels were assessed by RT-PCR.

We first asked whether the four identified cytoskeletal proteins participate in HIV-1 infection. We designed specific small interfering RNAs (siRNAs) to assess the impact of protein depletion on infection in single cycle infectivity assays. Multiple siRNAs were tested for each candidate, and the efficiency of knockdown was monitored by reverse transcription PCR. A pool of scramble siRNAs was used as the negative control. Expression of MAP1A, although predominant in the brain, was also detected in P4-CCR5 cells, human primary macrophages, and peripheral blood mononuclear cells and could be inhibited by specific siRNAs (Figs. 1 and 2). Depletion of MAP1A from infected cells led to a 10–20-fold decrease in the infectivity of both wild-type *env* and VSV-G-pseudotyped HIV-1 (Fig. 1). Similarly, knockdown of MAP1S led to a weaker but consistent (~5-fold) reduction of infectivity. The same infectivity profiles were observed with VSV-G-pseudotyped HIV-1 (Fig. 1*B*), indicating that viral entry via pH-dependent endocytosis, which results in a delivery of viral capsids deeper in the cytoplasm, does not alleviate the dependence of HIV-1 on MAPs for infection. In contrast, WIRE and CKAP1 depletion had no effect on HIV-1 infectivity, whether wild-type *env* or VSV-G-pseudotyped, despite strong knockdown levels (Fig. 1*B*). Using these single-cycle infectivity assays, we concluded that MAP1A and MAP1S play a role during the early steps of HIV-1 infection.

Having screened multiple siRNAs for each candidate for efficient knockdown (data not shown), we cloned the most efficient sequence as a small hairpin RNA in an HIV-1-derived lentiviral vector engineered to carry eGFP as the reporter gene (LV-shRNA) (Table 2). This provided controlled knockdown conditions and a straightforward readout for transduction efficiency for all subsequent RNAi experiments. Vectors were titered in target cells, and transductions were carried out at m.o.i. 50; knockdown was assessed by RT-PCR (Fig. 2*B*) and Western blotting (Fig. 2*C*). The effect of cytoskeletal protein depletion on cell viability was monitored by an MTT colorimetric assay, which measures mitochondrial activity in living cells. No statistically significant difference in viability was observed between any sample and the non-transduced (NT) control at 4 dpt when the measurements were made (Fig. 2*D*). Following infection of transduced cells, the same infectivity defects were observed with MAP1A (~10-fold) and MAP1S (~5-fold) shRNAs as previously with siRNAs, and similarly, CKAP1 and WIRE targeting shRNAs had no effect on HIV-1 infection, with wild-type *env* (Fig. 2*E*) and VSV-G-pseudotyped (Fig. 2*F*) HIV-1.

MAP1A and MAP1S Mediate the Ability of HIV-1 to Reach the Nucleus—Having shown that MAP1A and MAP1S contribute to the efficiency of HIV-1 infection in single-cycle infectivity assays, we sought to identify the specific step in which they are implicated. To assess whether MAP1 proteins affect reverse transcription, we quantified late reverse transcripts (LRT) in KD cells at 24 hpi. As controls, the cells were either transduced with LV-shLuc or non-transduced. The reverse transcription inhibitor nevirapine (5 μM) was also included. In independent experiments, no statistically significant difference in LRT levels was observed between any of the samples when compared with shLuc, indicating comparable efficiencies in reverse transcription (Fig. 3*A*). A previous study shows that two microtubule-associated proteins, DNAL1 and MAP4, impact HIV-1 reverse transcription when depleted (38). However, in two independent experiments, siRNA-mediated depletion of DNAL1 and MAP4 had no statistically significant effect on HIV-1 reverse transcription when compared with scramble control (Fig. 3*A*). MAP1A and MAP1S did not contribute to the reverse transcription efficiency of HIV-1, arguing that HIV-1 trafficking to the nuclear pore and reverse transcription are independent processes (11, 12).

To assess whether MAP1 proteins affect nuclear import or integration, we quantified 2-LTR circles, which are an exclusively nuclear form of viral DNA and can therefore be used as a marker of nuclear import. We found that both MAP1A and MAP1S depletion led to a reduction in 2-LTR circles in infected

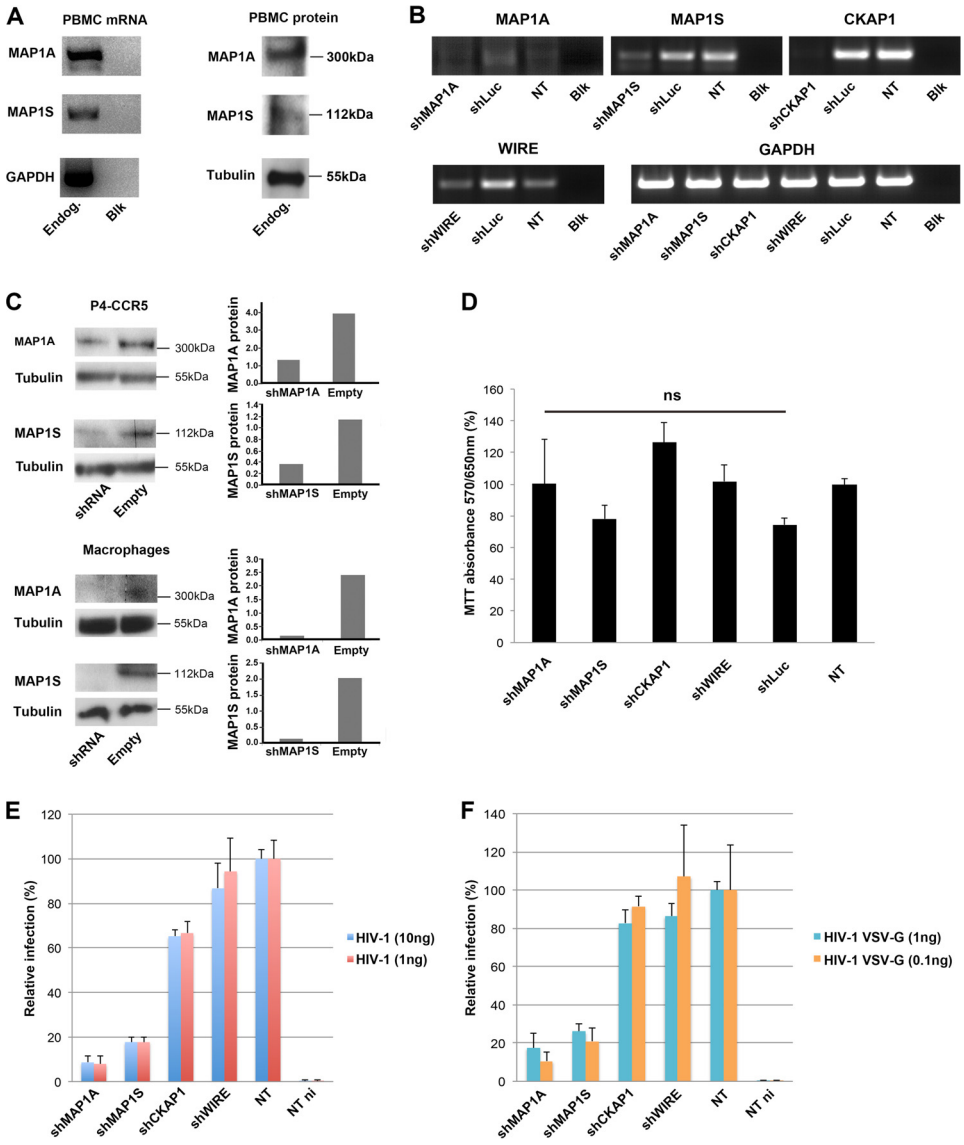

FIGURE 2. **shRNA-mediated depletion of MAP1A and MAP1S leads to a decrease in HIV-1 infection.** *A*, endogenous MAP1A and MAP1S transcripts and proteins were detected in human peripheral blood mononuclear cells (*PBMC*) from healthy blood donors by RT-PCR and Western blotting, respectively. For Western blotting, ~20 μg of protein was loaded per well, corresponding to ~150,000 peripheral blood mononuclear cells. *Blk*, PCR blank control. *B* and *C*, cells were transduced with shRNAs at m.o.i. 50. Knockdown efficiency was assessed at 3 dpt using RT-PCR (*B*) and Western blotting with quantification of protein bands (integrated optical density, arbitrary units) (*C*). The results are representative of three independent experiments. *D*, cell viability in shRNA-transduced P4-CCR5 cells was determined by detecting mitochondrial activity in living cells using the MTT assay. Results show the mean of two independent experiments carried out in triplicate ±S.D. *E* and *F*, transduced P4-CCR5 cells were infected either with HIV-1 (*E*) or VSV-G-pseudotyped HIV-1 (*F*). β-Galactosidase activity was measured at 2 days post-infection. Results show the mean of two independent experiments carried out in duplicate ±S.D. with NT controls set as 100%. For this point, raw values were ~400,000 relative light units/s on average.

cells at 24 hpi (2–4-fold), whereas WIRE and CKAP1 knockdown had no effect (Fig. 3*B*). This decrease was also seen when quantifying integrated HIV-1 proviruses by Alu-PCR (Fig. 3*C*), indicating a reproducible and statistically significant decrease in nuclear import. In the case of MAP1A, the measured defect in nuclear import was as low as expected when compared with the defect in infectivity. Indeed, we had noted previously that residual nuclear import (up to 10% of wild-type levels) is detected even for HIV-1 viruses that are unable to replicate in primary lymphocytes, regardless of the technique used to quantify nuclear viral DNA (Southern blotting or quantitative PCR) (39), which may account for an underestimation of the impact of MAP1A depletion on nuclear import.

Finally, we asked whether the depletion of MAP1 proteins leads to an overall defect in HIV-1 genome nuclear import or merely delays it, as might be expected to happen if viral trafficking could still occur without functional microtubular transport. We monitored 2-LTR circles over a 72-h time course post-infection. The proportional defect in the 2-LTR copy number remained the same in MAP1A- and MAP1S-depleted cells over the whole time course (Fig. 3*D*), indicating an overall defect in nuclear import rather than a delay.

MAP1A and MAP1S Mediate HIV-1 Trafficking to the Nuclear Membrane—Because MAP1A and MAP1S contribute to efficient HIV-1 nuclear access and are associated with microtubules, we asked whether MAP1 proteins might contribute to

TABLE 2
siRNA and shRNA sequences used in this study

MAP1A #1	CCUGAGCCAAAGGAUGAAGTT TTGGACUCGGUUUCCUACUUC
MAP1A #2	AAGCUUCGGCAUCUGGACUTT TTUUCGAAGCCGUAGACCUGA
MAP1S	GACUGAGAAAGAAGCCAAGTT TTCUGACUCUUUCUUCGGUUC
CKAP1	GGGAAACGCUACUUCGAAUTT TTCCCUUUGCGAUGAAGCUUA
WIRE #1	GUAUUCCUUCCAUCCAGUATT TTCAUAAGGAAGGUAGGUCAU
WIRE #2	GAGAACCUAGCUGGUAAGCTT TTCUCUUGGAUCGACCAUUCG
shMAP1A	AAGCTTCGGCATCTGGACTttcaagagaAGTCCAGATGCCGAAGCTTttttt
shMAP1S	GACTGAGAAAGAAGCCAAGttcaagagaCTTGGCTTCTTTCTCAGTCttttt
shCKAP1	GGGAAACGCTACTTCGAATttcaagagaATTCGAAGTAGCGTTTCCCttttt
shWIRE	GTATTCCTTCCATCCAGTAttcaagagaTACTGGATGGAAGGAATACttttt
shLuc	GTGCGTTGCTAGTACCAACttcaagagaGTTGGTACTAGCAACGCACttttt

efficient trafficking of incoming HIV-1 to the nuclear membrane. We labeled infected KD cells with an anti-p24 antibody at 8 hpi (m.o.i. ~50), a time point at which viral complexes have uncoated or are in the process of uncoating and entering the nucleus (26). Lower m.o.i. values (m.o.i. 1–5) have been used with similar results; however, they do not produce a sufficient capsid signal to allow statistical analysis. LV-shRNA transduction efficiency was monitored by GFP expression from the internal cassette. Image acquisition was performed using confocal microscopy of multiple z-stack images of random fields and analyzed using an Acapella script (Fig. 4*A*). Overall, less p24 labeling was observed in control samples (NT and shLuc), suggesting that uncoating has already been initiated. In contrast, MAP1A and MAP1S depletion led to an accumulation of p24 labeling throughout the cytoplasm, suggesting an inability both to reach the nuclear membrane and to uncoat (Fig. 4*B*). Particularly, in MAP1A KD cells, capsid labeling formed characteristic clumps scattered throughout the cytoplasm, away from the nucleus. A similar accumulation was not apparent in the case of CKAP1 and WIRE depletion. Acapella quantification revealed a statistically significant decrease in the number of perinuclear spots per cell volume and perinuclear spot density in the case of MAP1A depletion, indicating that MAP1A knockdown leads to a reduced presence of HIV-1 capsid in the perinuclear area, regardless of the cell volume or output measured (Fig. 4*C*).

To determine the earliest time point at which the absence of MAP1 proteins leads to a defect in HIV-1 trafficking and ascertain whether the defect persists with time, we performed a time course experiment by localizing the HIV-1 capsid signal at different time points post-infection in KD and control cells. We acquired images at 30 min and at 2, 4, 8, and 24 hpi. Results show that the defect in HIV-1 trafficking to the nuclear membrane is apparent in the absence of MAP1A and MAP1S as early as 4 hpi and persists at 24 hpi, indicating that the defect is not a delay but an impediment in trafficking (Fig. 5). The p24 signal observed throughout the cytoplasm of MAP-depleted cells at late time points post-infection suggests that complexes not only failed to traffic toward the nucleus but also had impaired uncoating. This may imply that complexes that fail to traffic to the nuclear pore, where the capsid can interact physically and functionally with nucleoporins and karyopherins, do not achieve proper uncoating. Alternatively, the p24 signal seen in MAP-depleted cells may be aggregates rather than individual cores, suggesting that a defect in trafficking to the nucleus may lead to core aggregation that might prevent efficient uncoating.

To confirm the implication of MAP1 proteins in HIV-1 trafficking in a physiological target cell of HIV-1, we knocked down their expression in primary macrophages. Knockdown was confirmed by Western blotting (Fig. 2*C*). Similarly to P4-CCR5 cells, depletion of MAP1A and MAP1S led to an accumulation of p24 signal in the cytoplasm (Fig. 6*A*), confirming that MAP1A and MAP1S contribute to efficient trafficking of HIV-1 to the nuclear membrane. To perform a statistical analysis of the capsid position in primary macrophages, which have lower culture density and permissiveness to infection than P4-CCR5 cells, we used a spinning disk confocal microscope combined with powerful Acapella scripts for high-throughput mosaic analysis (Fig. 4*A*). Because of the important number of fields acquired for each condition and the high performance computing required, we focused our analysis on MAP1S knockdown and control primary macrophages. We infected with HIV-1 primary macrophages transduced either with control or shMAP1S vector and labeled the infected cells for capsid localization. For each condition, 100 fields were acquired as non-overlapping z-stack mosaics in channels enabling the visualization of nuclei (Hoechst), transduced cells (GFP), and capsid. Acapella quantification revealed a statistically significant decrease in the number of perinuclear spots per cell volume, as well as perinuclear spot density in the case of MAP1S depletion, confirming in primary macrophages that MAP depletion leads to a reduced presence of HIV-1 capsid in the perinuclear area (Fig. 6*B*). Taken together, these experiments suggest that MAP1A and MAP1S contribute toward efficient trafficking of HIV-1 complexes toward the nucleus.

MAP1 Proteins Do Not Contribute toward Overall Cytoskeletal Architecture—To address how MAP1 proteins facilitate transport of HIV-1 RTCs to the nucleus, we first asked whether they affect the overall architecture of microtubule and microfilament networks, because loss of cytoskeletal network integrity would severely hamper infection. We labeled microtubules and microfilaments to assess their polymerization in KD cells and quantified cell morphology to test for possible structural collapse. No difference in cytoskeletal integrity was observed compared with non-transduced cells or shLuc-transduced cells (Fig. 7*A*), suggesting an underlying redundancy in the function of these proteins in the regulation of cytoskeletal polymerization. We noted, however, that WIRE-depleted cells were larger than control and other KD cells with an increased cytoplasmic volume of 65% but a constant nuclear volume (Fig. 7*B*). With the exception of this change, we concluded that the inhibition of HIV-1 infection following MAP1A/MAP1S depletion is not caused by the disruption of cytoskeletal trafficking that would result from an abnormal or depolymerized cytoskeleton.

MAP1A and MAP1S Contribute to Microtubule Stabilization in Primary Human Macrophages—Recent work has shown that HIV-1 infection induces, within 1–2 hpi, tubulin post-transla-

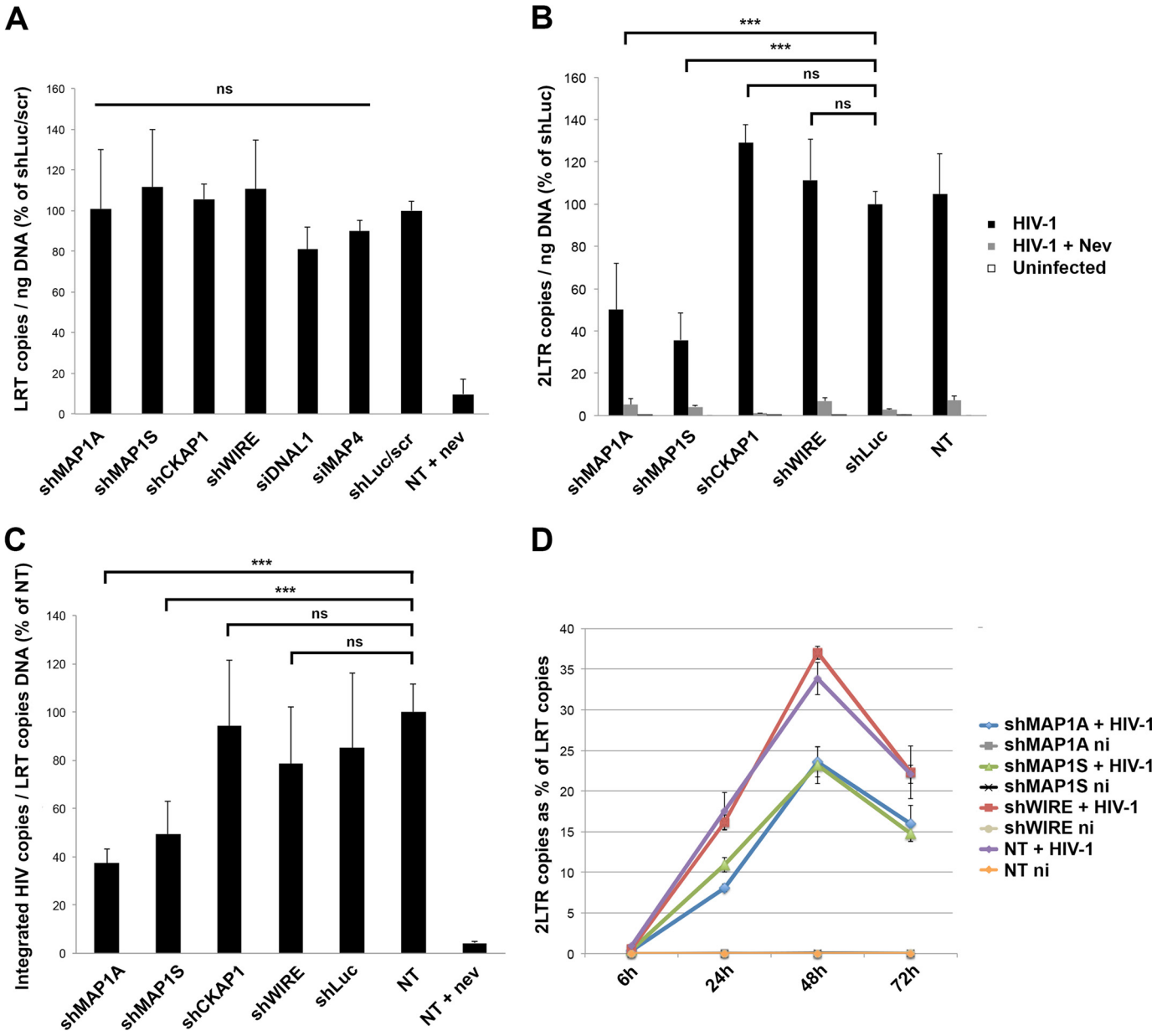

FIGURE 3. **Depletion of MAP1 proteins leads to an overall defect in nuclear access.** P4-CCR5 cells were transduced with shRNAs at m.o.i. 50 and infected with HIV-1 VSV-G at 3 dpt. *A–C*, at 24 hpi, DNA was extracted from infected cells, quantified, and subjected to quantitative PCR to assess LRT (*A*), 2-LTR circles (*B*), and integrated proviruses (*C*). The results shown are the mean of at least two independent experiments carried out in triplicate, expressed as a percentage of shLuc, scramble (*scr*), and NT control samples. Statistical significance was assessed by one-way ANOVA with multiple comparisons to control samples. *ns*, not significant. ***, $p < 0.001$. *D*, DNA was extracted from infected cells at given time points post-infection and subjected to 2-LTR and LRT PCR. The results show a representative experiment carried out in triplicate.

tional modifications that are associated with the formation of a more stable subset of microtubules, which facilitates the translocation of HIV particles across the cytoplasm (40). We therefore asked whether MAP1 proteins might promote microtubule stabilization in infected cells and thus facilitate overall retrograde trafficking of HIV-1. First, we tested the ability of HIV-1 to induce microtubule stability in primary macrophages, using as markers the prevalent post-translational modifications on stable microtubules, acetylation and detyrosination (41). Post-translational modifications characteristic of stable microtubules increased in primary human macrophages from three independent donors upon infection by both HIV-1 and VSV-G-pseudotyped HIV-1 (data not shown), ranging from 20 to 250% increase depending on experiments, a result concordant with previous findings (40) (Fig. 7*C*). Similarly, the protein levels of the microtubule plus end tracking protein (+TIP) EB1, which is required for microtubule stabilization and HIV-1 infection (40), were induced by HIV-1 infection (Fig. 7*C*).

As MAPs can alter the dynamic behavior of microtubules (35), we next asked whether MAP1A/MAP1S might contribute to microtubule stabilization. In both uninfected and infected cells, the knockdown of MAP1A and MAP1S led to a reproducible decrease in markers of stable microtubules by 2–3-fold on average, indicating that MAP1 proteins contribute, albeit modestly, to the stabilization of microtubules in primary human

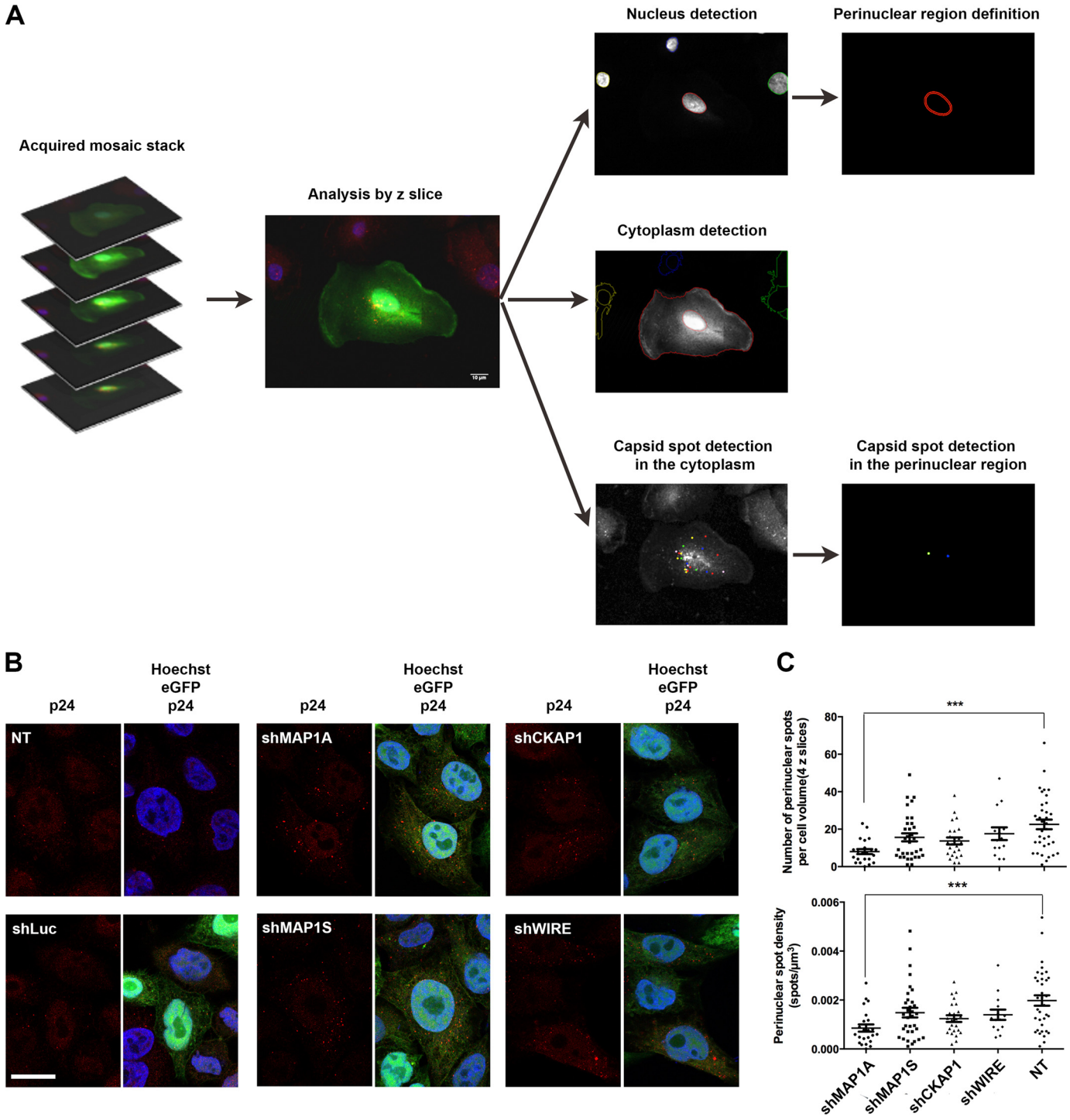

FIGURE 4. **MAP1 proteins contribute to efficient trafficking of HIV-1 RTC to the nuclear membrane.** *A*, algorithm overview for automatic capsid spot detection in perinuclear regions. The Acapella script was subdivided into three object subroutines segmenting successively the nucleus, the cytoplasm, and the capsid spots in the cytoplasm. From the nucleus border a mask was created with 1.2 μm thickness to define a perinuclear region in which the spots were counted. *Scale bar* indicates 10 μm. *B*, P4-CCR5 cells were transduced with shRNAs and infected with 100 ng of HIV-1 p24 (LAI) at 3 dpt. Infected cells were fixed at 8 hpi and labeled with anti-p24 antibodies. Images were acquired by LSM-700 confocal microscope. The *left panels* show the capsid signal, and the *right panels* show Hoechst, GFP (identifying transduced cells), and capsid superimposed. *Scale bar* indicates 10 μm. *C*, quantification of Acapella-detected perinuclear signal defined by two outputs: the number of perinuclear spots/constant number of z-slices (*top panel*) shows the number of spots in a given volume identical for all cells ($z = 4$); and the perinuclear spot density (*bottom panel*) shows the number of spots/μm^3, thus taking into account the cell volumes that are different for each cell. Each point corresponds to one random cell. Statistical significance was assessed using one-way ANOVA with Dunnett's multi-comparison test (***, $p \leq 0.001$).

macrophages (Fig. 7*C*). To determine whether the microtubule-stabilizing properties of MAP1 proteins could alone account for their impact on HIV-1 replication, we asked whether the infectivity defect observed in MAP1-depleted cells could be rescued in the presence of taxol, a drug that stabilizes microtubules and increases α-tubulin acetylation (42). LV-shRNA-transduced cells were

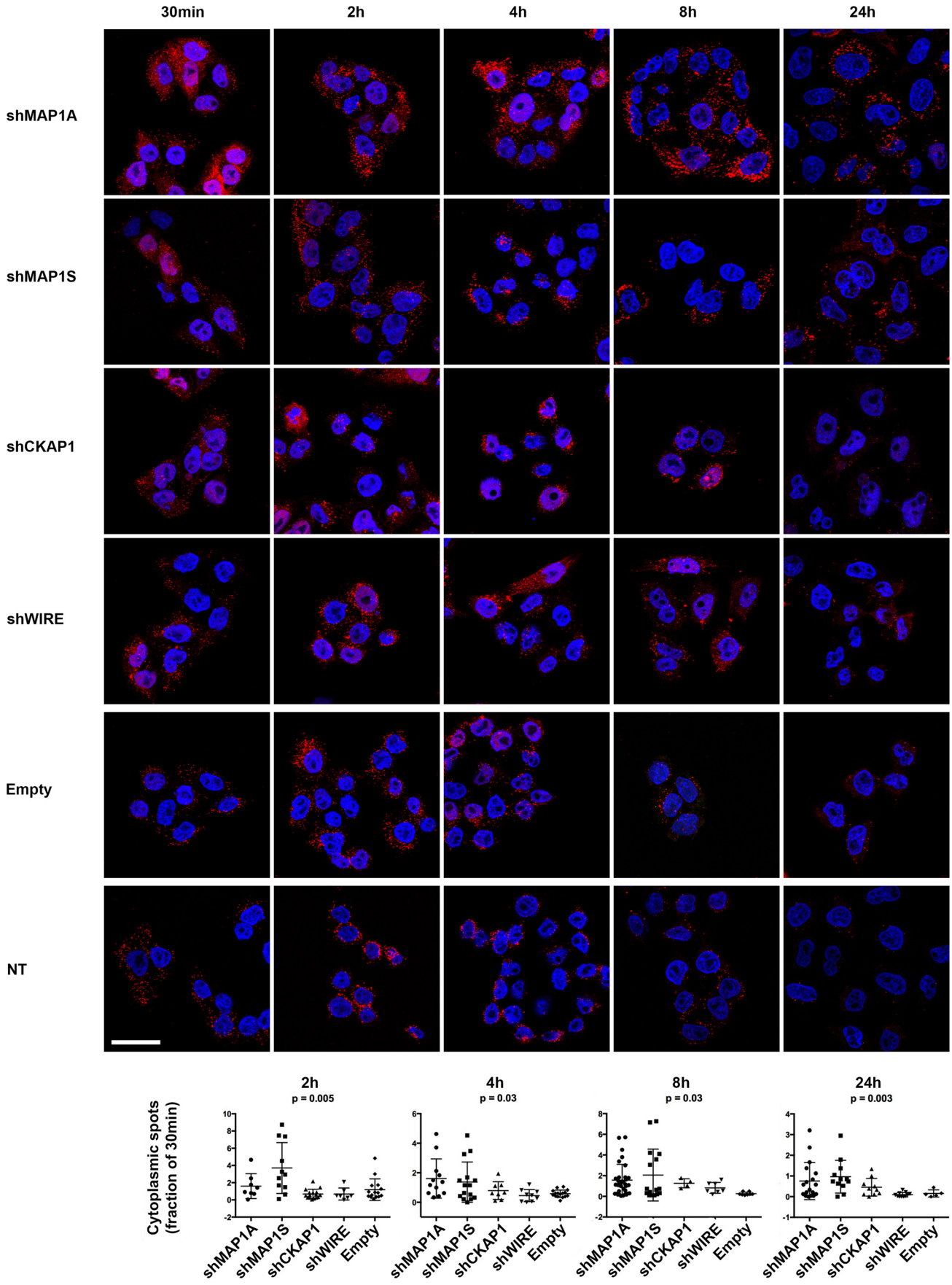
30min
2h
4h
8h
24h
shMAP1A
shMAP1S
shCKAP1
shWIRE
Empty
NT
Cytoplasmic spots (fraction of 30min)
2h
p = 0.005
4h
p = 0.03
8h
p = 0.03
24h
p = 0.003
shMAP1A
shMAP1S
shCKAP1
shWIRE
Empty

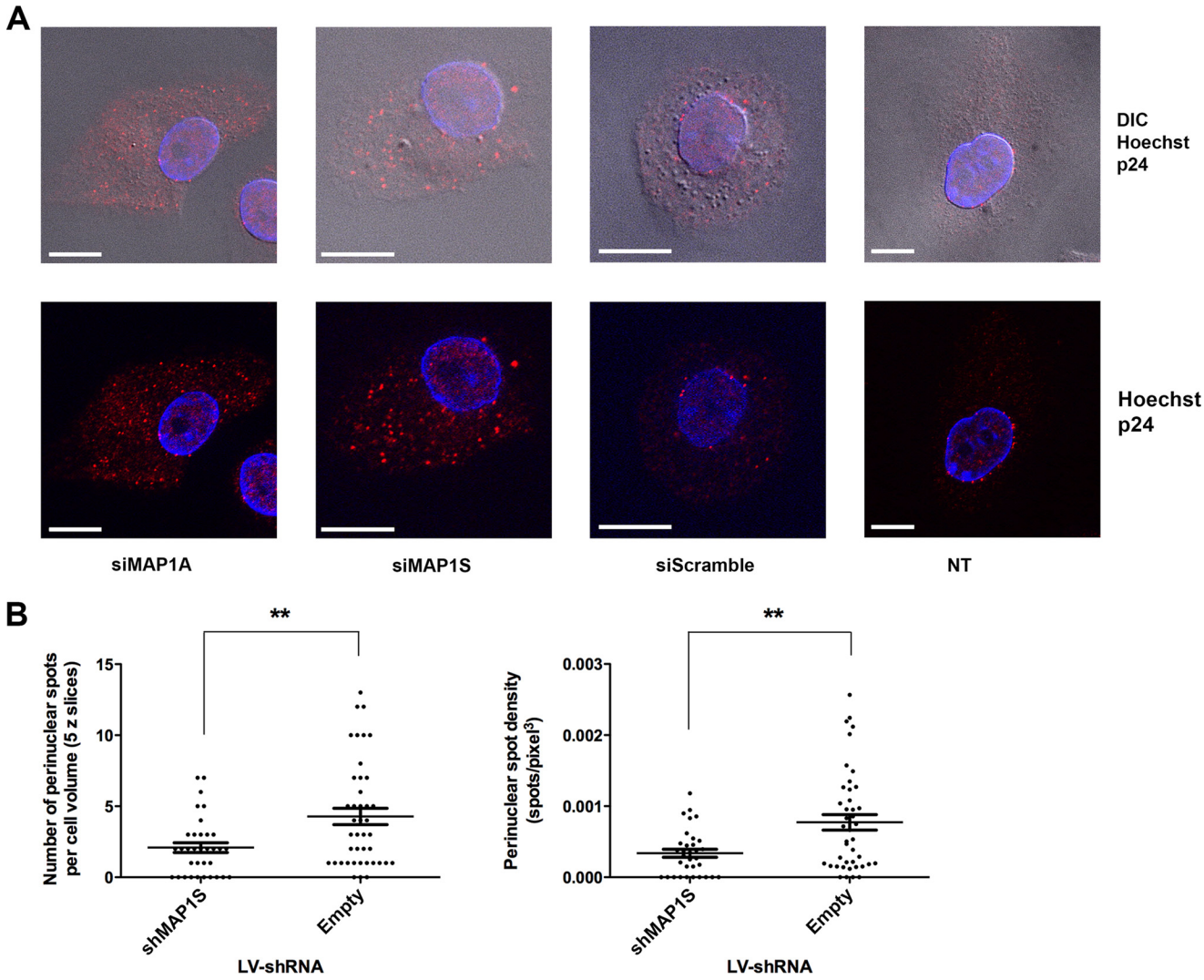

FIGURE 6. **MAP1 proteins contribute to efficient retrograde trafficking of HIV-1 in primary human macrophages.** *A*, macrophages were derived from blood monocytes by GM-CSF differentiation, lipofected with siRNAs against target candidates, and infected with HIV-1. Images were acquired using the Zeiss ApoTome, ×63 objective. *Scale bars* indicate 10 μm. *B*, transduced and infected primary macrophages were acquired using a Cell Voyager spinning disk confocal. Images were acquired for each condition in Hoechst, GFP (shRNA-transduced cells), and Cy3 (capsid labeling). Quantification of Acapella-detected perinuclear signal was performed as in *B*. Statistical significance was assessed using an unpaired *t* test (**, $p \leq 0.01$).

treated with increasing doses of taxol and infected with HIV-1. The results show that microtubule stabilization in the presence of taxol does not rescue infection in MAP1-depleted cells (Fig. 7*D*). Taken together, these results suggest that the ability of MAP1 proteins to stimulate the formation of stable microtubules is unlikely to contribute to retrograde trafficking of HIV-1.

HIV-1 Capsid Interacts with MAP1 Proteins—As MAP1 proteins were identified in yeast two-hybrid screens using p24 protein as bait, we next asked whether they might be able to bind to HIV-1 RTCs and thus mediate their association with microtubules. HIV-1 uncoating has been shown to occur within 30–45 min of infection (20, 29) or up to 4–12 h post-infection (11, 28) depending on studies and cell type, indicating that RTCs that latch onto the cytoskeleton in the minutes following cell entry still contain the capsid shell. The four candidate cytoskeletal protein coding sequences were cloned into pCi-Neo-3×FLAG plasmids for overexpression in 293T cells. In the case of MAP1A, the clones identified by our yeast two-hybrid screen all covered regions of the light chain, LC2, indicating that LC2 is the binding target of p24 (Table 1). This domain, which contains both microtubule and F-actin binding sequences, constitutes a good candidate based on our previous work that

FIGURE 5. **The defect in HIV-1 RTC trafficking to the nuclear membrane in the absence of MAP1 proteins is visible as early as 4 hpi and up to 24 hpi.** P4-CCR5 cells were transduced with shRNAs and infected with 100 ng of HIV-1 p24 (LAI) at 3 dpt. Infected cells were fixed at various times points post-infection (30 min and 2, 4, 8, and 24 h) and labeled with an anti-p24 antibody. Images were acquired using an LSM700 inverted microscope with a ×63 objective, no zoom, frame size 1024 × 1024 pixels, an average of two images, and scanning speed 9. The *panels* show Hoechst and capsid superimposed. *Scale bar* indicates 20 μm. The number of capsid spots/cell was quantified using Acapella as described in the legend for Fig. 4. Graphs represent the number of cytoplasmic spots after subtraction of spots detected in the perinuclear region, defined as a mask of 10-pixel thickness surrounding the nuclear membrane. Data are represented as fractions normalized for the number of cytoplasmic spots at 30 min, defined as the viral input for each condition ±S.D. Statistical analysis was calculated using non-parametric one-way ANOVA (Kruskal-Wallis). NT samples were not included in the analysis because the absence of GFP signal prevented cytoplasm detection (see Fig. 4*A*).

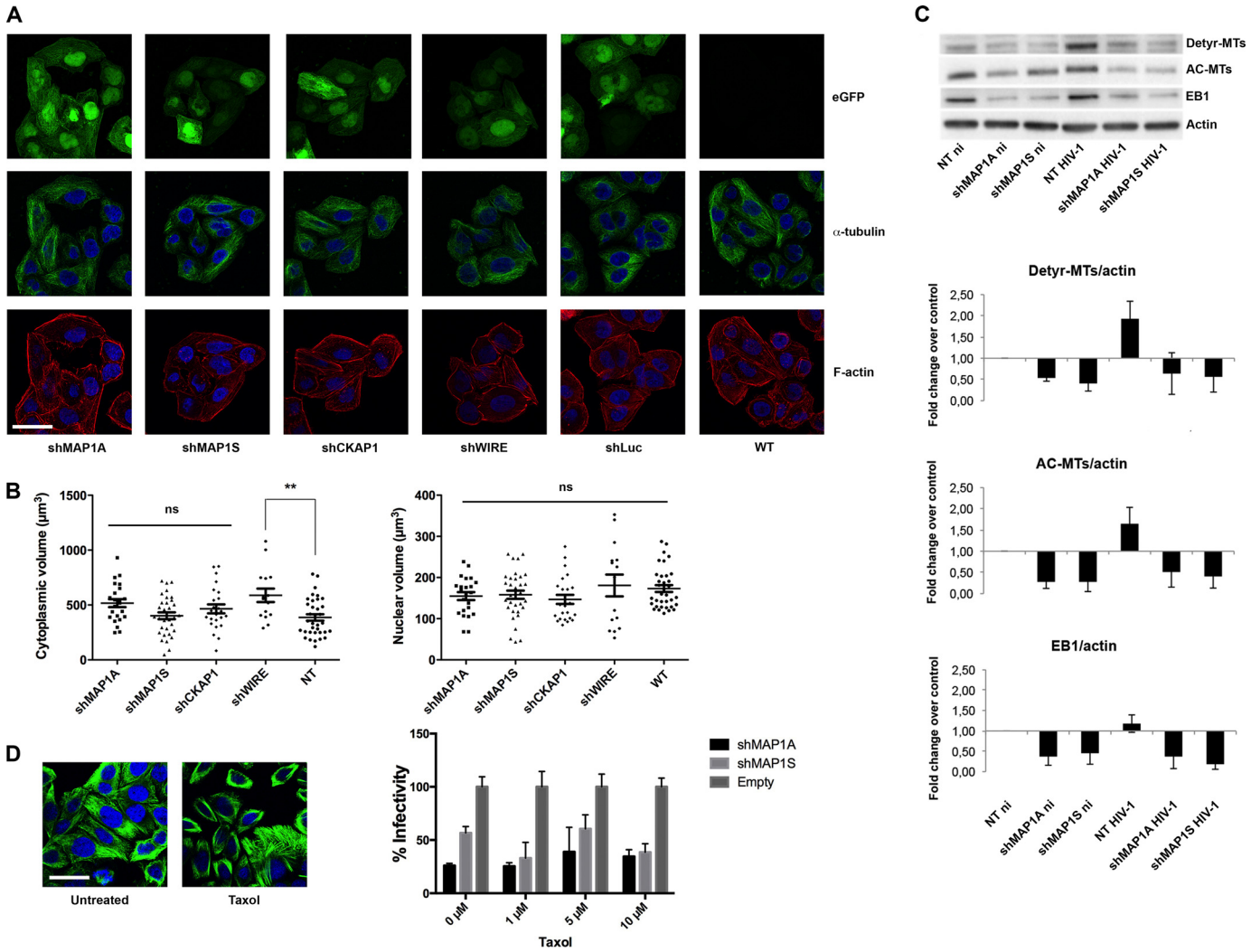

FIGURE 7. **MAP1A/MAP1S induce microtubule stabilization in primary human macrophages.** *A*, loss of MAP1A, MAP1S, CKAP1, and WIRE does not lead to a loss of cytoskeletal integrity. P4-CCR5 cells were transduced with shRNAs, fixed at 3 dpt, and labeled with anti-tubulin antibodies or rhodamine phalloidin. Images were acquired using an LSM700 inverted microscope. GFP expressed as a transgene from the LV-shRNA indicates transduction efficiency. *Scale bar* indicates 20 μm. *B*, quantification of Acapella-detected cell volume. Each point corresponds to one random cell and indicates the cytoplasm (*left panel*) and nucleus volume (*right panel*) in μm^3 for each analyzed cell, with mean ± S.E. Statistical analyses (one-way ANNOVA with Dunnett's multiple comparisons test) were performed using Prism 6 (GraphPad) (**, $p \leq 0.01$). *ns*, not significant. *C*, primary macrophages were transduced with shRNAs at m.o.i. 50 and infected with HIV-1. Cell extracts were prepared 6 hpi, and expression levels of AC-MT, detyr-MT and EB1 were analyzed by Western blotting. Actin was used as a loading control. Graphs show the mean quantification of protein bands (ImageJ) from five independent experiments in three different donors ±S.E. *D*, P4-CCR5 cells transduced with empty control or LV-shRNA were treated with increasing doses of taxol and infected with 5 ng of p24 HIV-1. Images show α-tubulin labeling in control and 1 μM Taxol-treated cells. Graph shows mean triplicate β-galactosidase values normalized by Bradford represented as a percentage of empty control ± S.E., representative of 2 independent experiments.

suggests that HIV-1 uses both microtubules and actin filaments for retrograde transport (3). We isolated HIV-1 cores using ultracentrifugation through a sucrose cushion in a protocol adapted from Shah and Aiken (43) and incubated them with cell lysates prepared from transfected 293T cells. To monitor for the nonspecific pulldown of proteins, lysates alone were ultracentrifuged without cores. The capsid-binding protein CypA was included as a positive control and the mRNA-binding protein hnRNP E1 as a negative control. The results showed a strong interaction for MAP1A-LC2 and MAP1S with isolated HIV-1 cores (Fig. 8*A*). A weaker interaction with CKAP1 and WIRE was also detected. These results indicate that both MAP1 proteins interact with the HIV-1 cores, suggesting that they can serve as anchor points on microtubules for HIV RTCs.

To confirm the interaction of HIV-1 capsid with MAP1A in infected cells, we performed a Duolink *in situ* proximity ligation assay. NT and shMAP1A-transduced cells, infected or not with HIV-1, were probed with anti-p24 and anti-MAP1A primary antibodies followed by species-specific proximity ligation assay probes. As expected, no signals were observed in uninfected control cells, and few signals were detected in the MAP1A-depleted cells. Our results show an interaction of MAP1A with viral capsid in HIV-1-infected cells, confirming the interaction at a cellular level in the context of infection (Fig. 8*B*). Similar results were obtained following infection with VSV-G-pseudotyped HIV-1 (data not shown).

MAP1 Proteins Help Tether HIV-1 Capsids to Microtubules—Because MAP1 proteins associate with both microtubules and HIV-1 capsid, we asked whether MAP1 proteins might mediate

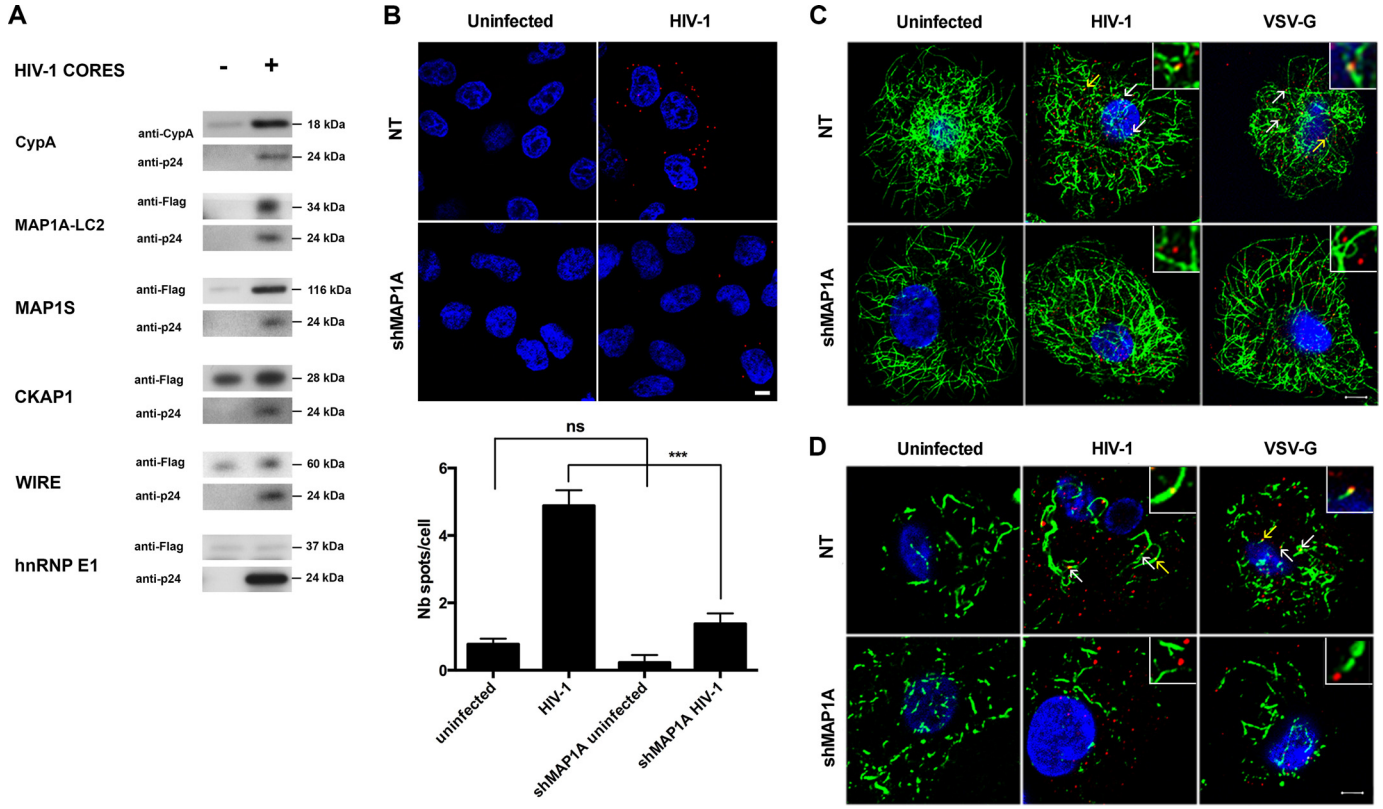

FIGURE 8. **MAP1A and MAP1S interact with HIV-1 cores.** *A*, MAP1A-LC2, MAP1S, CKAP1, and WIRE fused to a FLAG sequence were tested for interaction with HIV-1 capsids isolated after treatment of whole virions with low detergent concentrations. CypA and hnRNP E1 constituted positive and negative controls, respectively. *B*, p24 interacts with MAP1A in the cytoplasm of P4-CCR5 cells. P4-CCR5 cells were transduced with shMAP1A at m.o.i. 50 and infected with HIV-1. Protein interactions between p24 and MAP1A were detected by Duolink proximity ligation assay (*red dots*). *Scale bar* indicates 5 μm. Quantification was performed using Photoshop CS6 and statistical analyses using Prism 6 (GraphPad). Graph shows the average number of spots over the number of Hoechst-stained nuclei in five random fields/condition $\pm$S.E. (***, $p \leq 0.001$). *ns*, not significant. *C* and *D*, primary macrophages were transduced with shMAP1A at m.o.i. 50 and infected with HIV-1 and VSV-G-pseudotyped HIV-1. Cells were fixed at 6 hpi and triple-stained with the DNA-specific probe Hoechst (*blue*), rabbit polyclonal anti-p24 antibodies (*red*), and a mouse monoclonal anti-α-tubulin (*C*) or acetylated tubulin (*green*) (*D*). Images show representative data. In control cells, the *arrows* indicate proximity events between HIV-1 capsid and microtubules, and examples highlighted by *yellow arrows* are magnified in *insets*. *Scale bar* indicates 5 μm.

the interaction between HIV-1 capsids and microtubules. We labeled infected cells with p24 antibody and probed for co-localization with both dynamic and stable microtubules. Close proximity events, highlighted by a yellow signal where green and red channels overlap, were readily observed in control infected cells, indicating that HIV-1 cores can associate with both dynamic (Fig. 8*C*) and stable microtubules (Fig. 8*D*). In contrast, the proximity of capsid and microtubules was rarely observed in MAP1A-depleted cells, suggesting that capsids overlap less well with microtubules in the absence of MAP1 proteins (Fig. 8, *C* and *D*). Similar results were obtained following infection with VSV-G-pseudotyped HIV-1 (Fig. 8, *C* and *D*). Taken together, our results support a model in which MAP1 proteins promote HIV-1 retrograde trafficking by tethering HIV-1 capsids to microtubules.

DISCUSSION

After cell entry, HIV-1 is propelled toward the nucleus by cytoskeleton-directed trafficking (44). Although trafficking along microtubules has been characterized in terms of velocity and movement dynamics (2, 3), the nature of the interactions between the HIV RTC and the host cytoskeleton that mediate retrograde trafficking are relatively unknown. This study reports the importance of microtubule-associated proteins MAP1A and MAP1S for efficient HIV-1 infection and retrograde trafficking. We found that MAP1 proteins interact with HIV-1 cores *in vitro* and in infected cells and that depletion of MAP1 proteins reduces the association of HIV-1 capsids with both dynamic and stable microtubules. Taken together, our data suggest that MAP1 proteins help tether incoming viral capsids to the microtubular network, thus promoting cytoplasmic trafficking.

MAP1 proteins bind along the length of microtubules, and an *in situ* proximity ligation assay showed the association of HIV-1 capsid and MAP1 proteins throughout the cell cytoplasm, suggesting that interaction with MAP1 proteins is likely to occur repeatedly during transport along microtubules and not just as an initial latching onto the cytoskeleton at the cell periphery. We showed previously that HIV-1-directed transport along microtubules toward the nucleus is saltatory (3). Intermittent transport along microtubules suggests binding to and detachment from filaments. MAP1 proteins may provide important anchor points for HIV-1 complexes traveling toward the nucleus, enabling reattachment following dissociation.

Following infection, HIV-1 complexes undergo uncoating (loss of capsid) prior to nuclear entry. Some uncoating or partial uncoating occurs in early post-infection in the cell periphery.

However the importance of capsid for efficient reverse transcription, as well as its presence deep in the cytoplasm and at the nuclear pore, implies that many complexes that traffic along the cytoskeleton toward the nucleus still contain capsid. Our work suggests that the viral structure that interacts with the cytoskeleton for trafficking to the nucleus is the viral capsid protein.

MAP1 proteins are thought to stabilize microtubules by altering their intrinsic dynamic instability (35). Here, MAP1 did not impact microtubule network integrity or cell morphology but contributed to microtubule stabilization, which was shown previously to facilitate infection (40). Therefore, although the contribution of MAP1 to microtubule stabilization is modest in primary human macrophages, it is likely that their ability to promote microtubule stabilization also contributes to their overall effect on HIV-1 trafficking.

The cytoskeletal proteins CKAP1 and WIRE, which are two other potential candidates identified as HIV-1 p24 binding partners in the yeast two-hybrid screen, were not found to be involved in the early phases of infection. This study does not exclude their involvement in the later phases of the cycle or redundancy with other family proteins for their function.

Evidence suggests that HIV-1 trafficking may involve both microtubules and microfilaments (2, 3, 45, 46). The importance of both actin filaments and microtubules for HIV-1 infection has also been highlighted by a series of siRNA genome-wide screens for cellular factors necessary for infection (4–6), which identified a number of proteins that regulate the polymerization and stability of microfilaments (*e.g.* gelsolin, spectrin, and cofilin) and microtubules (*e.g.* calpain, microtubule-associated protein, and kinesin superfamily proteins). Interestingly, MAPs have been reported to facilitate microtubule-actin cross-talk, and the interaction of HIV-1 cores with MAP1A is mediated by its light chain, LC2, which contains both microtubule and microfilament binding domains. Therefore, MAP1A and MAP1S, in which the light chains are 39% homologous, may be involved in the transition between the actin cortex and microtubules immediately following cell entry or between microtubules and microfilaments around the nuclear membrane before docking at the nuclear pore (3). Indeed, an inability to engage onto microfilaments might result in an anterograde movement back toward the periphery, which might account for the scattering of HIV-1 complexes that we observed throughout the cytoplasm in KD cells.

Alternatively, MAPs have been reported to interact with molecular motors and interfere directly with microtubule or cargo binding or affect their overall function (47). Although MAP1A and MAP1S can localize along the length of microtubules, the different localization densities of MAP1A and MAP1S along microtubular tracks (47) suggest that they might participate in cargo engagement onto microtubules at the cell periphery or in the drop-off of cargo by molecular motors near the nuclear membrane. Although the molecular motor(s) involved in HIV-1 retrograde trafficking has not yet been identified, evidence suggests that dynein might be involved; treatment with the dominant negative inhibitor p150 CC1 domain of dynactin, which uncouples dynein-based transport, or microinjection of anti-dynein antibodies leads to a clustering of HIV-1 in the cell periphery (2, 3, 48). Moreover, the detected speeds and directionality of incoming HIV-1 (>1 μm/s (3)) suggest dynein-mediated microtubular movement. In the case of spumaviruses, a direct interaction between human foamy virus Gag and LC8, the light chain of dynein, has been demonstrated (48), although another study suggests that interaction with LC8 might be involved in other cellular processes and thus not be specific for retrograde transport (49). No molecular motors were identified in our yeast two-hybrid screen. This could be because of the sheer size and complexity of molecular motors; dynein, for instance, comprises two heavy chains, three intermediate chains, and four light chains and typically functions in conjunction with the dynactin complex, which consists of at least 10 additional proteins. Moreover, because movement is bidirectional (3), it is possible that incoming complexes simultaneously bind to molecular motors of opposite polarity, as has been shown for the herpes simplex virus HSV-1 (50).

Cargo loading onto microtubule tracks, navigation along its route, and subsequent cargo delivery are likely to be regulated by multiple, interdependent mechanisms, such as microtubule polarity, post-translational modifications, and microtubule-associated proteins (47). Our results and previous studies together suggest that HIV-1 may also use multiple mechanisms to regulate its retrograde transport, such as interaction with minus end-directed motors, induction of stable microtubules, and interaction with microtubule-associated proteins (Refs. 40 and 51 and this study).

Taken together, our work reveals that HIV-1 cores interact with MAP1 proteins for trafficking to the nucleus, leading to efficient nuclear import and infection. Further work will shed light on how these proteins participate in the trafficking dynamics and transitions among microtubules, microfilaments, and nuclear pores.

REFERENCES

1. Radtke, K., Döhner, K., and Sodeik, B. (2006) Viral interactions with the cytoskeleton: a hitchhiker's guide to the cell. *Cell Microbiol.* **8,** 387–400
2. McDonald, D., Vodicka, M. A., Lucero, G., Svitkina, T. M., Borisy, G. G., Emerman, M., and Hope, T. J. (2002) Visualization of the intracellular behavior of HIV in living cells. *J. Cell Biol.* **159,** 441–452
3. Arhel, N., Genovesio, A., Kim, K. A., Miko, S., Perret, E., Olivo-Marin, J. C., Shorte, S., and Charneau, P. (2006) Quantitative four-dimensional tracking of cytoplasmic and nuclear HIV-1 complexes. *Nat. Methods* **3,** 817–824
4. Brass, A. L., Dykxhoorn, D. M., Benita, Y., Yan, N., Engelman, A., Xavier, R. J., Lieberman, J., and Elledge, S. J. (2008) Identification of host proteins required for HIV infection through a functional genomic screen. *Science* **319,** 921–926
5. König, R., Zhou, Y., Elleder, D., Diamond, T. L., Bonamy, G. M., Irelan, J. T., Chiang, C. Y., Tu, B. P., De Jesus, P. D., Lilley, C. E., Seidel, S., Opaluch, A. M., Caldwell, J. S., Weitzman, M. D., Kuhen, K. L., Bandyopadhyay, S., Ideker, T., Orth, A. P., Miraglia, L. J., Bushman, F. D., Young, J. A., and Chanda, S. K. (2008) Global analysis of host-pathogen interactions that regulate early-stage HIV-1 replication. *Cell* **135,** 49–60
6. Zhou, H., Xu, M., Huang, Q., Gates, A. T., Zhang, X. D., Castle, J. C., Stec, E., Ferrer, M., Strulovici, B., Hazuda, D. J., and Espeseth, A. S. (2008) Genome-scale RNAi screen for host factors required for HIV replication. *Cell Host Microbe* **4,** 495–504
7. Dismuke, D. J., and Aiken, C. (2006) Evidence for a functional link between uncoating of the human immunodeficiency virus type 1 core and nuclear import of the viral preintegration complex. *J. Virol.* **80,** 3712–3720
8. Yamashita, M., Perez, O., Hope, T. J., and Emerman, M. (2007) Evidence

for direct involvement of the capsid protein in HIV infection of nondividing cells. *PLoS Pathog.* **3,** 1502–1510
9. Yamashita, M., and Emerman, M. (2004) Capsid is a dominant determinant of retrovirus infectivity in nondividing cells. *J. Virol.* **78,** 5670–5678
10. Krishnan, L., Matreyek, K. A., Oztop, I., Lee, K., Tipper, C. H., Li, X., Dar, M. J., Kewalramani, V. N., and Engelman, A. (2010) The requirement for cellular transportin 3 (TNPO3 or TRN-SR2) during infection maps to human immunodeficiency virus type 1 capsid and not integrase. *J. Virol.* **84,** 397–406
11. Arhel, N. J., Souquere-Besse, S., Munier, S., Souque, P., Guadagnini, S., Rutherford, S., Prévost, M. C., Allen, T. D., and Charneau, P. (2007) HIV-1 DNA Flap formation promotes uncoating of the pre-integration complex at the nuclear pore. *EMBO J.* **26,** 3025–3037
12. Di Nunzio, F., Danckaert, A., Fricke, T., Perez, P., Fernandez, J., Perret, E., Roux, P., Shorte, S., Charneau, P., Diaz-Griffero, F., and Arhel, N. J. (2012) Human nucleoporins promote HIV-1 docking at the nuclear pore, nuclear import, and integration. *PLoS One* **7,** e46037
13. Schaller, T., Ocwieja, K. E., Rasaiyaah, J., Price, A. J., Brady, T. L., Roth, S. L., Hué, S., Fletcher, A. J., Lee, K., KewalRamani, V. N., Noursadeghi, M., Jenner, R. G., James, L. C., Bushman, F. D., and Towers, G. J. (2011) HIV-1 capsid-cyclophilin interactions determine nuclear import pathway, integration targeting, and replication efficiency. *PLoS Pathog.* **7,** e1002439
14. Stremlau, M., Perron, M., Lee, M., Li, Y., Song, B., Javanbakht, H., Diaz-Griffero, F., Anderson, D. J., Sundquist, W. I., and Sodroski, J. (2006) Specific recognition and accelerated uncoating of retroviral capsids by the TRIM5α restriction factor. *Proc. Natl. Acad. Sci. U.S.A.* **103,** 5514–5519
15. Perron, M. J., Stremlau, M., Lee, M., Javanbakht, H., Song, B., and Sodroski, J. (2007) The human TRIM5α restriction factor mediates accelerated uncoating of the *N*-tropic murine leukemia virus capsid. *J. Virol.* **81,** 2138–2148
16. Black, L. R., and Aiken, C. (2010) TRIM5α disrupts the structure of assembled HIV-1 capsid complexes *in vitro*. *J. Virol.* **84,** 6564–6569
17. Roa, A., Hayashi, F., Yang, Y., Lienlaf, M., Zhou, J., Shi, J., Watanabe, S., Kigawa, T., Yokoyama, S., Aiken, C., and Diaz-Griffero, F. (2012) RING domain mutations uncouple TRIM5α restriction of HIV-1 from inhibition of reverse transcription and acceleration of uncoating. *J. Virol.* **86,** 1717–1727
18. Forshey, B. M., von Schwedler, U., Sundquist, W. I., and Aiken, C. (2002) Formation of a human immunodeficiency virus type 1 core of optimal stability is crucial for viral replication. *J. Virol.* **76,** 5667–5677
19. Brun, S., Solignat, M., Gay, B., Bernard, E., Chaloin, L., Fenard, D., Devaux, C., Chazal, N., and Briant, L. (2008) VSV-G pseudotyping rescues HIV-1 CA mutations that impair core assembly or stability. *Retrovirology* **5,** 57
20. Hulme, A. E., Perez, O., and Hope, T. J. (2011) Complementary assays reveal a relationship between HIV-1 uncoating and reverse transcription. *Proc. Natl. Acad. Sci. U.S.A.* **108,** 9975–9980
21. Rasaiyaah, J., Tan, C. P., Fletcher, A. J., Price, A. J., Blondeau, C., Hilditch, L., Jacques, D. A., Selwood, D. L., James, L. C., Noursadeghi, M., and Towers, G. J. (2013) HIV-1 evades innate immune recognition through specific cofactor recruitment. *Nature* **503,** 402–405
22. Lahaye, X., Satoh, T., Gentili, M., Cerboni, S., Conrad, C., Hurbain, I., El Marjou, A., Lacabaratz, C., Lelièvre, J. D., and Manel, N. (2013) The capsids of HIV-1 and HIV-2 determine immune detection of the viral cDNA by the innate sensor cGAS in dendritic cells. *Immunity* **39,** 1132–1142
23. Goujon, C., Moncorgé, O., Bauby, H., Doyle, T., Ward, C. C., Schaller, T., Hué, S., Barclay, W. S., Schulz, R., and Malim, M. H. (2013) Human MX2 is an interferon-induced post-entry inhibitor of HIV-1 infection. *Nature* **502,** 559–562
24. Kane, M., Yadav, S. S., Bitzegeio, J., Kutluay, S. B., Zang, T., Wilson, S. J., Schoggins, J. W., Rice, C. M., Yamashita, M., Hatziioannou, T., and Bieniasz, P. D. (2013) MX2 is an interferon-induced inhibitor of HIV-1 infection. *Nature* **502,** 563–566
25. Liu, Z., Pan, Q., Ding, S., Qian, J., Xu, F., Zhou, J., Cen, S., Guo, F., and Liang, C. (2013) The interferon-inducible MxB protein inhibits HIV-1 infection. *Cell Host Microbe* **14,** 398–410
26. Kim, S. Y., Byrn, R., Groopman, J., and Baltimore, D. (1989) Temporal aspects of DNA and RNA synthesis during human immunodeficiency virus infection: evidence for differential gene expression. *J. Virol.* **63,** 3708–3713
27. Barbosa, P., Charneau, P., Dumey, N., and Clavel, F. (1994) Kinetic analysis of HIV-1 early replicative steps in a coculture system. *AIDS Res. Hum. Retroviruses* **10,** 53–59
28. Arfi, V., Lienard, J., Nguyen, X. N., Berger, G., Rigal, D., Darlix, J. L., and Cimarelli, A. (2009) Characterization of the behavior of functional viral genomes during the early steps of human immunodeficiency virus type 1 infection. *J. Virol.* **83,** 7524–7535
29. Warrilow, D., Tachedjian, G., and Harrich, D. (2009) Maturation of the HIV reverse transcription complex: putting the jigsaw together. *Rev. Med. Virol.* **19,** 324–337
30. Charneau, P., Mirambeau, G., Roux, P., Paulous, S., Buc, H., and Clavel, F. (1994) HIV-1 reverse transcription: a termination step at the center of the genome. *J. Mol. Biol.* **241,** 651–662
31. Yee, J. K., Miyanohara, A., LaPorte, P., Bouic, K., Burns, J. C., and Friedmann, T. (1994) A general method for the generation of high-titer, pantropic retroviral vectors: highly efficient infection of primary hepatocytes. *Proc. Natl. Acad. Sci. U.S.A.* **91,** 9564–9568
32. Zennou, V., Petit, C., Guetard, D., Nerhbass, U., Montagnier, L., and Charneau, P. (2000) HIV-1 genome nuclear import is mediated by a central DNA flap. *Cell* **101,** 173–185
33. Butler, S. L., Hansen, M. S., and Bushman, F. D. (2001) A quantitative assay for HIV DNA integration *in vivo*. *Nat. Med.* **7,** 631–634
34. Brussel, A., and Sonigo, P. (2003) Analysis of early human immunodeficiency virus type 1 DNA synthesis by use of a new sensitive assay for quantifying integrated provirus. *J. Virol.* **77,** 10119–10124
35. Halpain, S., and Dehmelt, L. (2006) The MAP1 family of microtubule-associated proteins. *Genome Biol.* **7,** 224
36. Grynberg, M., Jaroszewski, L., and Godzik, A. (2003) Domain analysis of the tubulin cofactor system: a model for tubulin folding and dimerization. *BMC Bioinformatics* **4,** 46
37. Takenawa, T., and Suetsugu, S. (2007) The WASP-WAVE protein network: connecting the membrane to the cytoskeleton. *Nat. Rev. Mol. Cell Biol.* **8,** 37–48
38. Gallo, D. E., and Hope, T. J. (2012) Knockdown of MAP4 and DNAL1 produces a post-fusion and pre-nuclear translocation impairment in HIV-1 replication. *Virology* **422,** 13–21
39. Iglesias, C., Ringeard, M., Di Nunzio, F., Fernandez, J., Gaudin, R., Souque, P., Charneau, P., and Arhel, N. (2011) Residual HIV-1 DNA Flap-independent nuclear import of cPPT/CTS double mutant viruses does not support spreading infection. *Retrovirology* **8,** 92
40. Sabo, Y., Walsh, D., Barry, D. S., Tinaztepe, S., de Los Santos, K., Goff, S. P., Gundersen, G. G., and Naghavi, M. H. (2013) HIV-1 induces the formation of stable microtubules to enhance early infection. *Cell Host Microbe* **14,** 535–546
41. Janke, C., and Bulinski, J. C. (2011) Post-translational regulation of the microtubule cytoskeleton: mechanisms and functions. *Nat. Rev. Mol. Cell Biol.* **12,** 773–786
42. Piperno, G., LeDizet, M., and Chang, X. J. (1987) Microtubules containing acetylated α-tubulin in mammalian cells in culture. *J. Cell Biol.* **104,** 289–302
43. Shah, V. B., and Aiken, C. (2011) *In vitro* uncoating of HIV-1 cores. *J. Vis. Exp. 2011,* e3384
44. Brandenburg, B., and Zhuang, X. (2007) Virus trafficking: learning from single-virus tracking. *Nat. Rev. Microbiol.* **5,** 197–208
45. Zamborlini, A., Lehmann-Che, J., Clave, E., Giron, M. L., Tobaly-Tapiero, J., Roingeard, P., Emiliani, S., Toubert, A., de Thé, H., and Saïb, A. (2007) Centrosomal pre-integration latency of HIV-1 in quiescent cells. *Retrovirology* **4,** 63
46. Yoder, A., Guo, J., Yu, D., Cui, Z., Zhang, X. E., and Wu, Y. (2011) Effects of microtubule modulators on HIV-1 infection of transformed and resting CD4 T cells. *J. Virol.* **85,** 3020–3024
47. Atherton, J., Houdusse, A., and Moores, C. (2013) MAPping out distribution routes for kinesin couriers. *Biol. Cell* **105,** 465–487
48. Petit, C., Giron, M. L., Tobaly-Tapiero, J., Bittoun, P., Real, E., Jacob, Y., Tordo, N., De The, H., and Saib, A. (2003) Targeting of incoming retrovi-

ral Gag to the centrosome involves a direct interaction with the dynein light chain 8. *J. Cell Sci.* **116,** 3433–3442
49. Tan, G. S., Preuss, M. A., Williams, J. C., and Schnell, M. J. (2007) The dynein light chain 8 binding motif of rabies virus phosphoprotein promotes efficient viral transcription. *Proc. Natl. Acad. Sci. U.S.A.* **104,** 7229–7234
50. Radtke, K., Kieneke, D., Wolfstein, A., Michael, K., Steffen, W., Scholz, T., Karger, A., and Sodeik, B. (2010) Plus- and minus-end directed microtubule motors bind simultaneously to herpes simplex virus capsids using different inner tegument structures. *PLoS Pathog.* **6,** e1000991
51. Gaudin, R., de Alencar, B. C., Arhel, N., and Benaroch, P. (2013) HIV trafficking in host cells: motors wanted! *Trends Cell Biol.* **23,** 652–662